Supplementary Information (SI) for Green Chemistry.

Supplementary Information

for

An environmentally degradable Al-air battery to realize future green energy-matter flow

Jinrui Li,[#,a] *Yunhao Xu,*[#,a] *Senlin Wei,*[a] *Cheng Tong,**[*,a] *Minhua Shao,*[b,c] *Cunpu Li,**[*,a] *and Zidong Wei*[a]

a. State Key Laboratory of Advanced Chemical Power Sources, School of Chemistry and Chemical Engineering, Chongqing University, Chongqing, 400044, China.

b. Department of Chemical and Biological Engineering, Hong Kong University of Science and Technology, Clear Water Bay, Kowloon, Hong Kong, 999077, China.

c. Guangzhou Key Laboratory of Electrochemical Energy Storage Technologies, Fok Ying Tung Research Institute, The Hong Kong University of Science and Technology, Guangzhou 511458, China.

#. Jinrui Li and Yunhao Xu contributed equally to this work.

** Corresponding authors. E-mail: tongcheng@cqu.edu.cn (C. Tong); lcp@cqu.edu.cn (C. Li).*

1. Experimental section

1.1 Chemicals

Hemin (Adamas, 98%), norbornylene (NBE) (Aladdin, 99%), Grubbs II (Adamas, 97%), trichloromethane ($CHCl_3$) (Aladdin, 99%), polyvinyl alcohol (PVA) (Adamas, 98%), acrylic acid (AA) (Adamas, 99%), ammonium persulphate (APS) (Adamas, 99.9%), potassium hydroxide (KOH) (Adamas, ≥90.0%), ethanol (Adamas, 99.9%), Al sheet (Changsha Spring, 99.9%), carbon paper (Changsha Spring). All solutions were prepared using deionized water ($18\ M\Omega\ cm^{-1}$). N_2 (99.999%), O_2 (99.995%) and H_2 (99.999%) were purchased from Chongqing Ruisin Gas Industry.

1.2 Material synthesis

1.2.1 Synthesis of the Poly(NBE-*co*-Hemin) catalyst

0.05 mmol hemin, 0.5 mol norbornylene, and 0.001 g Grubbs II catalyst were dissolved in 25 mL trichloromethane in a round-bottom flask by ultrasound. Then the mixture was heated at 45°C with stirring and stored in a dark environment for 24 hours. Then, the sample was washed three times with ethanol, and then dried in an oven at 90°C for 24h to obtain the Poly(NBE-*co*-Hemin) catalyst. To prepare the cathode, the catalyst was ground into powder and then dispersed in proper amount of alcohol (1 mg Poly(NBE-*co*-Hemin) catalyst in 1 mL alcohol). Then the as-prepared Poly(NBE-*co*-Hemin) catalyst dispersion was sprayed on a carbon paper and dried at 90°C for 5 h to obtain the cathode.

1.2.2 Synthesis of the PVA-AA-6M KOH hydrogel electrolyte

2 g polyvinyl alcohol was dissolved in deionized water at 95°C and stirred at 1000 r/min for 1 hour. 2 g acrylic monomer was then added into the solution and the solution was stirred for 60 min. 0.1 g ammonium persulfate was then added into the solution as an initiator for agitation with stirring. After 10 min, the solution was transferred to a glass plate and stood for 2 h at 90°C till the solution turned into a film named PVA-AA. After cooling down to room temperature, PVA-AA was immersed in

6M KOH solution for 4 h to yield the final PVA-AA-6M KOH solid hydrogel electrolyte.

1.3 Material characterization

1.3.1 X-ray diffraction (XRD)

XRD patterns of the Poly(NBE-*co*-Hemin) catalyst, hemin, and PVA-AA-6M KOH hydrogel electrolyte were performed on a Shimadzu X-ray diffractometer (Model 6000) at a scanning rate of 5.7° min^{-1}.

1.3.2 Scanning electron microscope

The morphologies of the Poly(NBE-*co*-Hemin) catalyst and the PVA-AA hydrogel were observed using a scanning electron microscope (SEM, ZEISS Gemini 300 and FEI Nova400) at a voltage of 5 kV.

1.3.3 Fourier Transform infrared spectroscopy(FTIR)

FTIR of the Poly(NBE-*co*-Hemin) catalyst and hemin were performed by a FTIR spectrometer (Nicolet iS50) within the range of 4000 to 400 cm^{-1}.

1.3.4 Thermogravimetry Analysis(TGA)

TGA of Poly(NBE-*co*-Hemin) catalyst, hemin, PVA-AA hydrogel, and PVA-AA-6M KOH hydrogel electrolyte were conducted by a thermal gravimetric analyzer(TGA/DSC/1600LF) from Mettler-Toledo under N_2 atmosphere (flow rate of 50 mL min^{-1}) within the temperature range of 20 to 600°C.

1.3.5 Stress-strain test

The Stress-strain test of the PVA-AA hydrogel and the PVA-AA-6M KOH hydrogel electrolyte were performed by a material testing machine (MTS, E44.104) at a speed of 10 mm min^{-1}.

1.4 Electrochemical characterization

1.4.1 Rotating disk electrode (RDE) test

The ORR reaction under alkaline condition can be divided into a direct $4e^-$ transfer pathway and a stepwise $2e^-$ transfer pathway.

The direct $4e^-$ transfer pathway proceeds as follows:

$$O_2 + 4e^- + 2H_2O \rightarrow 4OH^- \quad (1)$$

The $2e^-$ reaction pathway is:

$$O_2 + 2e^- + H_2O \rightarrow OH^- + HO_2^- \quad (2)$$

$$HO_2^- + H_2O + 2e^- \rightarrow 3OH^- \quad (3)$$

HO_2^- then decomposes to hydroxide (OH^-) and O_2:

$$2HO_2^- \rightarrow 2OH^- + O_2 \quad (4)$$

In a system where two-electron transfer and four-electron transfer basically occur, the dominant relationship needs to be discerned. If the system is dominated by four-electron transfer, a higher power density is provided. In addition, the peroxide produced by the reaction can have a corrosive effect on the electrode device. Therefore, figuring out the pathway of the reaction is necessary to study the reaction process and the application of catalysts.

1.4.2 ORR performance test

In order to characterize the activity of the catalyst, an ORR performance test is required. The test was carried out in a three-electrode system. The three-electrode system used a saturated calomel electrode (Ag/AgCl electrode in the neutral system) as the reference electrode, a carbon rod as the counter electrode, and a glassy carbon electrode coated with the Poly(NBE-*co*-hemin) catalyst (4 mg of catalyst was weighed and dispersed in 400 µl of ethanol, 5 µl of nafion was added to disperse the catalyst well, and 7.9 µl of catalytic ink was applied to the glassy carbon electrode with a 20 µl pipette gun in a uniform manner) as the working electrode. The tests were carried out in 0.1 M KOH at a controlled temperature of 30 °C under N_2 conditions for 30 cycles of activation at a sweep rate of 50 mV s^{-1}, and after the catalyst activation was completed, the linear voltammetric sweep curves were scanned at a sweep rate of 10 mV S^{-1}. The linear voltammetric scanning were tested at different rotating speeds (400 rpm, 600 rpm, 800 rpm, 1000 rpm, 1200 rpm, 1400 rpm, 1600 rpm) under saturated O_2 conditions. The electron transfer number of the ORR was calculated from the Koutechy-Levich (K-L) equation:

$$\frac{1}{j} = \frac{1}{j_k} + \frac{1}{j_d} + \frac{1}{j_f} \quad (5)$$

In real case, the value of j_f is so large that this tends to 0 in the K-L equation and can be ignored, and the K-L equation can be abbreviated as:

$$\frac{1}{j} = \frac{1}{j_k} + \frac{1}{j_d} \quad (6)$$

The equation $j_d = B\omega^{0.5}$, $B = 0.62nFC_0D_0^{2/3}v^{-1/6}$, where F is Faraday's constant, which is 96485 C mol^{-1}, C_0 is the concentration of oxygen in the solution, with a magnitude C_0 is the concentration of oxygen in the solution with a magnitude of 1.2×10^{-3} mol cm^{-3}, D_0 is the diffusion rate of oxygen molecules in the solution with a value of 1.9×10^{-5} cm^2 s^{-1}, v is the kinetic viscosity of the solution, and the kinetic viscosity of 0.1 M KOH is 0.01 cm^2 s^{-1}, and n is the number of electron transferred. Bringing in all data, ω taking rad s^{-1} can be derived under alkaline condition:

$$B = 0.11n(\text{mA cm}^{-2}\ S^{\frac{1}{2}}) \quad (7)$$

K=1/B=1/(0.11n), n=1/(0.11K), K is the slope of the linear fit.

1.4.3 The Rotating Ring Disk Electrode (RRDE) test

The rotating ring-disk electrode is structurally similar to the ring-disk electrode except that a concentric ring is placed in the same plane on the periphery of the disk electrode, and an insulating substrate is used to separate the disk from the ring.

In the rotating ring-disk electrode, the disk current and ring current reflect the percentage of the four-electron process and two-electron process in the total reaction process, respectively, from which the hydrogen peroxide yield can be obtained and the number of electrons transferred can be calculated, with the specific formula as follows:

$$X_{HO_2^-} = \frac{200I_R/N}{I_D + I_R/N} \quad (8)$$

$$n = \frac{4I_D}{I_D + I_R/N} \quad (9)$$

ID and IR denote disk current and ring current, respectively, and N is a constant in this test (0.37).

1.4.4 Liquid-flow Al-air battery performance test

Assembling of the liquid flow battery: a certain amount of catalyst was weighed, dispersed with ethanol by ultrasound and then sprayed on a 2cm×2cm carbon paper to form a catalytic layer, and the loading amount of catalyst on the carbon paper was controlled to be 1 mg cm^{-2}. The catalyst-coated side of the carbon paper was placed against the hydrogel electrolyte in the middle, and the back side was placed with a piece of nickel foam as a fluid collector. The polished Al sheet was placed on the other side of the electrolyte as the negative electrode of the Al-air battery. The screws were tightened to prevent leakage, while adding the required electrolyte solution to the circulation pump and connecting the rubber hoses in the order of top in and bottom out. After assembling the battery device, the polarization curve test was carried out on a P4000 electrochemical workstation using a two-electrode system (the working electrode connected to the positive electrode, and the reference electrode and the counter electrode connected to the negative electrode) in an O_2 atmosphere. The voltage range was set within 0-1.8 V and the scanning speed was 0.1 mV S^{-1} to obtain the polarization curves and power density curves of the cells. Finally, the battery was discharged on the Land-CT2001A device under air atmosphere, and the test items were cross-current discharge test, gradient discharge test, and battery capacity test.

1.4.5 Al-Air Battery Pack Performance Test

The solid-state Al-air battery pack is a symmetric sandwich-like structure. Stacked together in the order of nickel foam, carbon paper (with sprayed catalyst), hydrogel electrolyte, and Al sheet, and secured with clamps, the polarization curves were measured on a P400 electrochemical workstation, under O_2 conditions, and the parameters tested were the same as those tested with the liquid Al-air battery. The discharge test was conducted on Land-CT2001A equipment under air condition.

The formula is based on the consumption of Al sheet. I denotes the current density throughout the constant-current discharge process, t represents the duration of the constant current discharge, and m signifies the mass of Al sheet consumed during the discharge process.

$$\mathrm{C} = \mathrm{It}/\mathrm{m} \quad (10)$$

2. Theoretical Calculation

2.1 Density function theory (DFT) calculation

Gaussian 2016 software[1] was used to optimize the structure of hemin anion. The chosen basis set was 6-311G(d). The single occupied molecular orbitals (SOMO) of hemin anion and O_2 were illustrated with the software VMD (version 1.9.4).[2]

2.2 Coarse-grained molecular dynamics method by material studio (MS)

Coarse-grained molecular dynamics (CGMD) simulations were performed with the GROMACS software package (version 2018.3) in this work.[3] The Martini II force field[4-6] was used to study the interactions of beads and the Amorphous Cell module was used to construct a polymer chain box. The mesoscale module was used to transform the relaxed all-atom model into a coarse-grained model. In this transformation, each monomer of the hemin-based polymer was treated as a single bead, while hydroxide ions, water molecules, and potassium ions were treated as three separate types of beads. The initial coarse-grained model was obtained and further optimized at a mesoscale level. The box had a side length of 77.5 Å. The Geometry Optimization module of force field was employed to optimize the structure. The convergence criteria were set as follows: energy convergence threshold of $2.0e^{-5}$ kcal/mol, force convergence threshold of 0.001 kcal/mol/Å, displacement convergence threshold of $1.0e^{-5}$ Å, and a maximum of 500 iterations, ensuring the system reached its minimum energy state. The system was balanced at a temperature of 298.15 K and a pressure of 1.013 MPa. The time step was set to 40 fs, with a total of 500,000 steps, resulting in a total equilibration time of 20,000 ps. Trajectory snapshots were output every 1,000 steps.

For the dynamically stable state, analysis was used to calculate the radial distribution function (RDF) between hydroxide ions and the polymer.[7-8] The cutoff distance was set to be 50 Å, and the distance interval was set to be 0.05 Å to compute the radial distribution function.

The radial distribution function (RDF) was calculated according to equation 1:

$$g(r)_{A-B} = \frac{dn_r}{4\pi dr\rho} \quad (11)$$

where ρ is the bulk density of B particles, and dn_r is the number of particles within a shell of thickness dr around particle A.

Supporting figures and tables

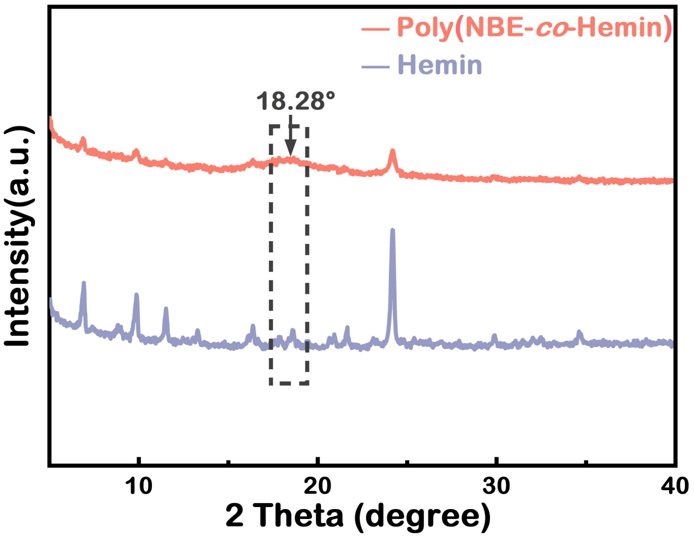

Figure S1. XRD patterns of the Poly(NBE-*co*-Hemin) catalyst and hemin.

The broad peak at 18.28° indicates successful polymerization of hemin and norbornylene.

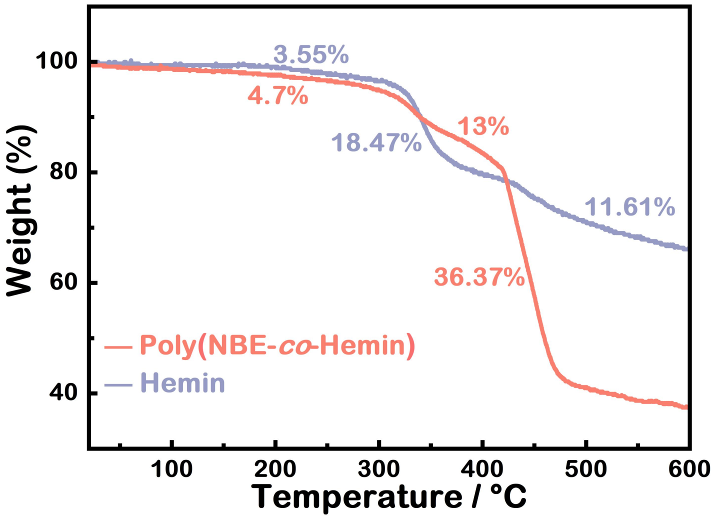

Figure S2. TGA curves of the Poly(NBE-*co*-Hemin) catalyst and hemin at a heating rate of 5°C min^{-1}.

Thermogravimetric analysis (TGA) was employed to analyze the components of the composite catalyst and three distinct stages are revealed as shown in Figure S2: the first stage from 20°C to 300°C is ascribed to the small molecules decomposition; the subsequent stage from 300°C to 420°C corresponds to the decomposition of functional groups in hemin, during which Poly(NBE-*co*-Hemin) decomposed at a slower rate due to the ring-opening metathesis polymerization (ROMP) reaction; the third stage from 420°C to 600°C is associated with dehydrogenation and breaking of the porphyrin ring, alongside the catalyst polymer degradation.

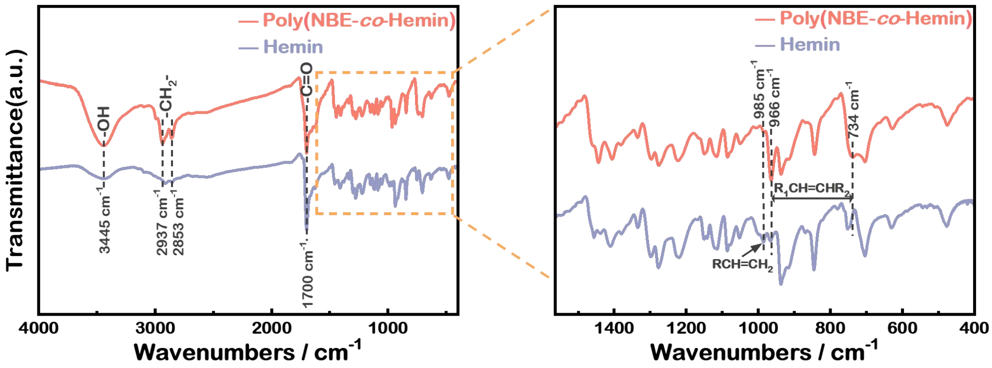

Figure S3. FTIR spectra of the Poly(NBE-*co*-Hemin) catalyst and hemin.

Molecular structures of the Poly(NBE-*co*-hemin) catalyst and hemin were analyzed using Fourier Transform Infrared Spectroscopy (FTIR). As illustrated in Figure S3**,** Poly(NBE-*co*-Hemin) and hemin exhibit comparable stretching vibration peaks of the functional group region. The peak observed at 3445 cm^{-1} is attributed to the stretching vibration of -OH. Additionally, the peaks at 2853 cm^{-1} and 2937 cm^{-1} correspond to the asymmetric stretching vibration of -CH_2 and the peaks at 1698 cm^{-1} are attributed to the stretching vibration of the -C=O in carboxylic acids. Furthermore, as depicted in the partially magnified spectrum (right part of Figure S3), notable =CH_2 bending vibration absorption peaks are observed at 985 cm^{-1} and 966 cm^{-1} due to $RHC=CH_2$ in hemin, while these stretching vibrations are less obvious in the Poly(NBE-*co*-Hemin) catalyst. In contrast, the more pronounced peak at 966 cm^{-1} is attributed to the newly formed $R_1HC=CHR_2$ in Poly(NBE-*co*-Hemin).

The X-Ray Diffraction (XRD) patterns presented in **Figure S1** and the Fourier Transform Infrared Spectroscopy (FTIR) in **Figure S3** prove hemin underwent a metathetic ring-opening polymerization reaction with norbornene to successfully synthesize the Poly(NBE-*co*-Hemin) catalyst.

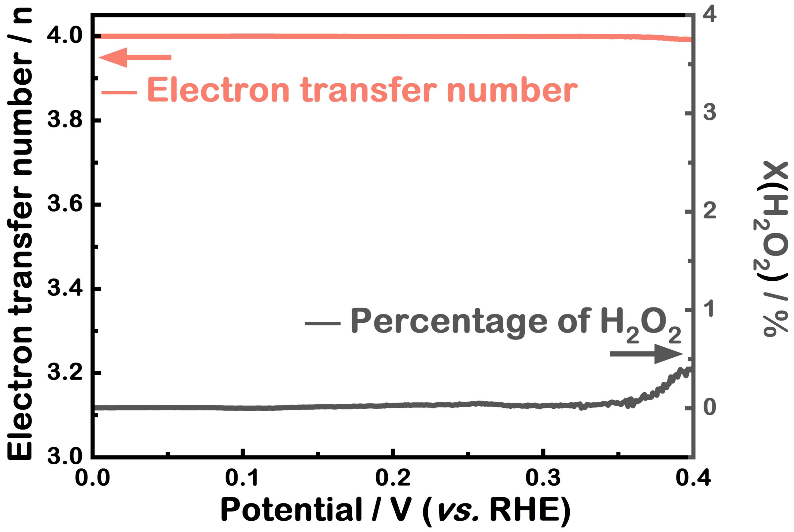

Figure S4. Electron transfer number of the cathode using the Poly(NBE-*co*-hemin) catalyst in 0.1M KOH and pure O_2 condition.

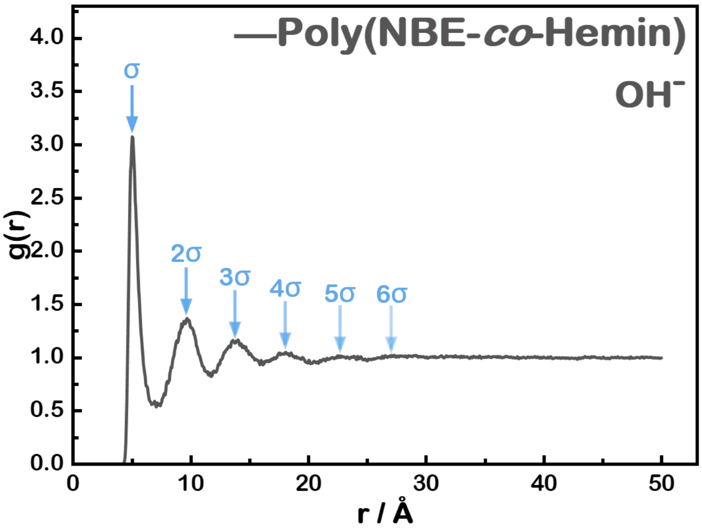

Figure S5. Radial distribution function (RDF) of OH^- in the Poly(NBE-*co*-hemin) catalyst calculated from the coarse grained molecular dynamics (CGMD).

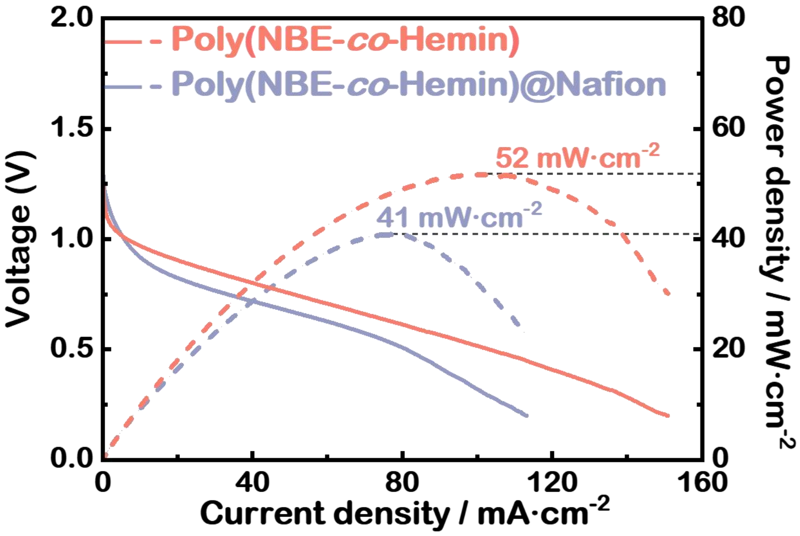

Figure S6. Current-voltage-power curves of the Al-air batteries using the Poly(NBE-*co*-Hemin) catalyst and Poly(NBE-*co*-Hemin)@Nafion catalyst, respectively, under 6 M KOH aqueous solution and air.

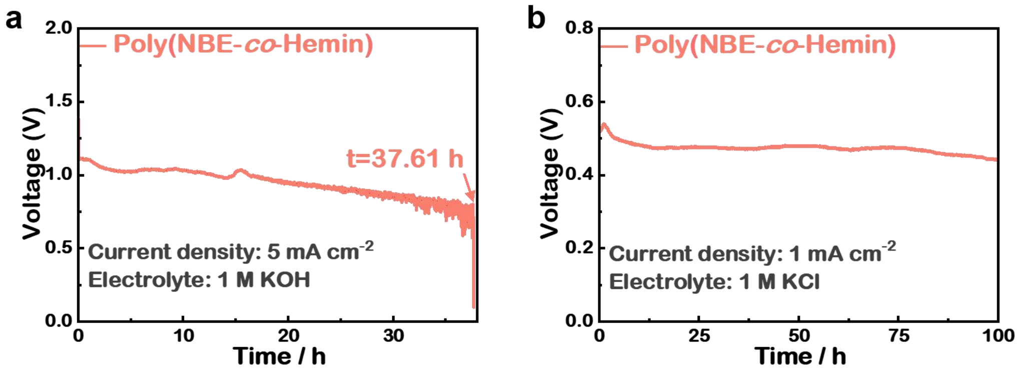

Figure S7. (a) Discharge time of the Poly(NBE-*co*-Hemin) catalyst battery in 1 M KOH aqueous solution and air. (b) Discharge time of the Poly(NBE-*co*-Hemin) catalyst battery in 1 M KCl aqueous solution and air.

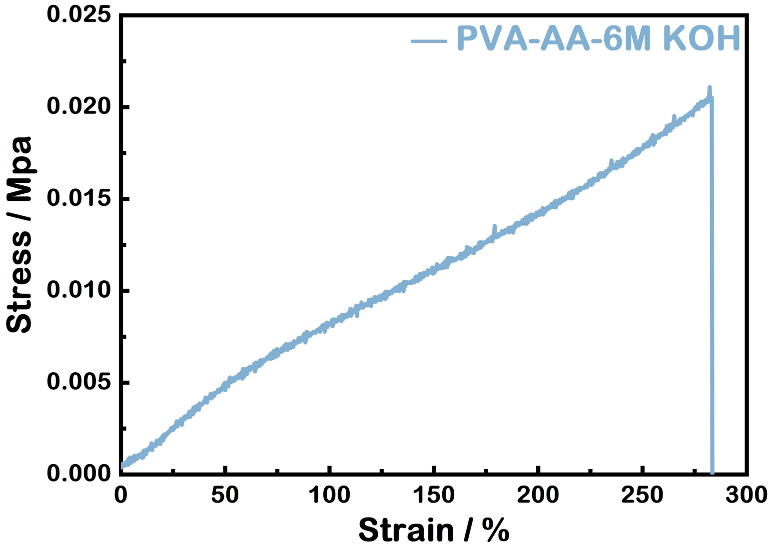

Figure S8. Tensile-strain curve of the PVA-AA-6M KOH hydrogel electrolyte.

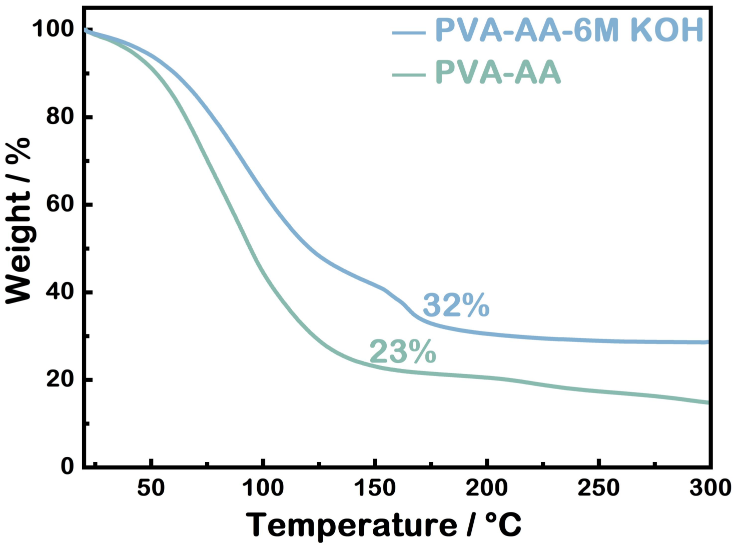

Figure S9. TGA curves of the PVA-AA-6M KOH electrolyte and the PVA-AA hydrogel.

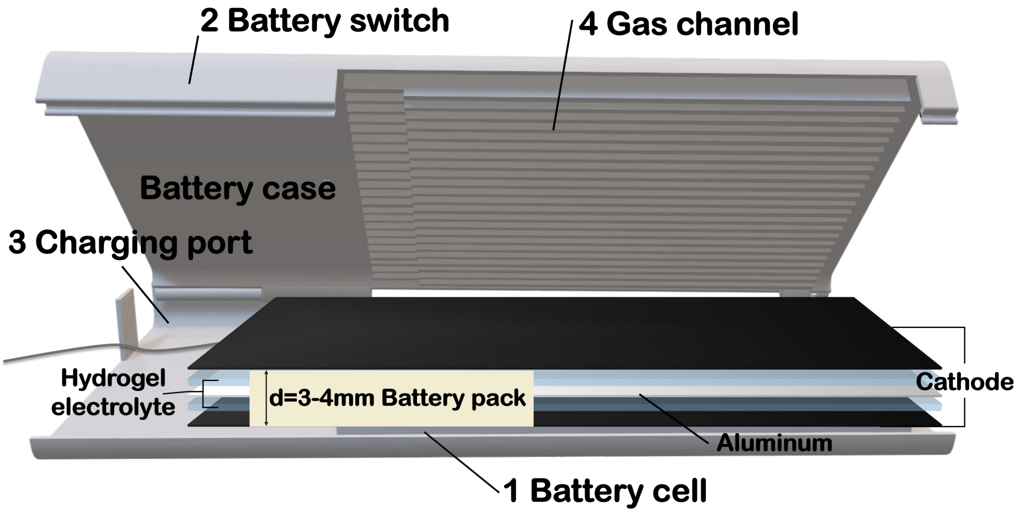

Figure S10. Schematic diagram of the practical degradable Al-air battery.

The battery pack consists of symmetrically stacked cathodes (with sprayed catalyst), Al sheet, and hydrogel electrolytes. Structure 1 represents the battery cell and structure 2 is the battery switch with a snap. When the battery case is secured by the snap, the resulting positive pressure enhances the contact between the cathode with sprayed Poly(NBE-*co*-Hemin) catalyst and the solid electrolyte interfaces. Structure 3 serves as the energy output port, specifically designed for connecting to device charging cables and structure 4 comprises a sawtooth plate grid, which functions as the gas flow channel.

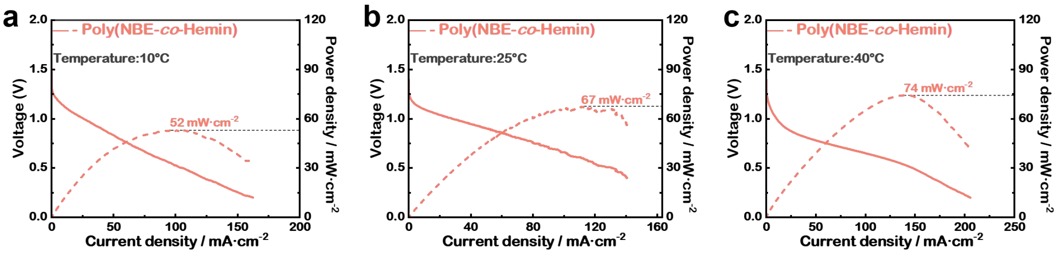

Figure S11. (a)-(c) Current-voltage-power curves of the Al-air batteries using the Poly(NBE-*co*-Hemin) catalyst and PVA-AA-6M KOH hydrogel electrolyte under air condition and gradient temperatures.

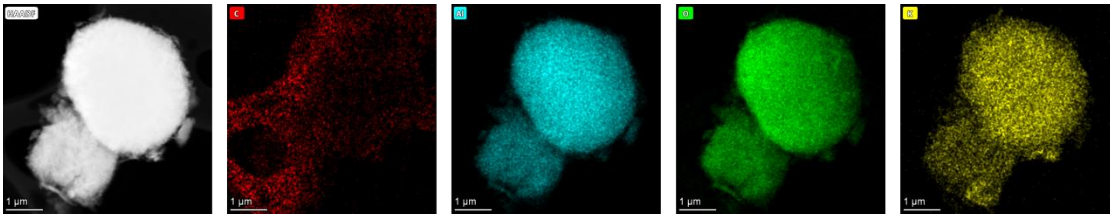

Figure S12. EDS elemental mapping of the PVA-AA-6M hydrogel electrolyte after discharge with HAADF-STEM.

Table S1. Discharge duration of Al-air batteries using Poly(NBE-*co*-Hemin) catalyst and hydrogel electrolytes made with different cross-linkers.

	Cross linker	Discharge time/h
PVA	**Acrylic Acid**	4.03
	Poly(Ethylene Glycol)	0.70
	polyethleneoxide	1.18
	D-$C_6H_{12}O_7$	0.20
	2-Hydroxypropionic Acid	1.33

Table S2. Mass of the degradable Al-air battery components and corresponding energy densities.

Component		**Mass**
Cathode	**Polymer catalyst**	0.07g
	Carbon	0.13 g
Hydrogel electrolyte		23.00g
Anode (Al)		7.56g
Total mass		30.76 g
Energy density		1022.40Wh kg^{-1}
Deliver energy density		231.79Wh kg^{-1}

Table S3. Prices of principal constituent materials for the designed Poly(NBE-*co*-Hemin) catalyst/PVA-AA-6M KOH hydrogel electrolyte system and the commercial 20%Pt/C catalyst/aqueous KOH electrolyte system in Al-air batteries with equivalent energy storage capacity.

	Component		Price / USD	Brand	Total price / USD
Poly(NBE-*co*-Hemin) +PVA-AA-6M KOH	**Catalyst**	**Hemin**	0.0055	Adamas	0.1774
		NBE	0.0122	Aladdin	
	Electrolyte	**PVA**	0.0901	Adamas	
		AA	0.0409	Adamas	
		KOH	0.0287	Greagent	
Commercial	**Catalyst**	**20%Pt/C**	1.1881	Adamas	1.2168
	Electrolyte	**KOH**	0.0287	Greagent	

Table S4. Prices of the designed Al-air battery and cost comparison with a commercial rechargeable battery.

Types of batteries	Production cost/ kWh electricity	Environmental friendliness
Our work	**25.5**	**√**
Lead-acid cell	**60**[9]	**Heavy metal (Pb)**
Lithium-ion battery	**94.5**[10]	**Fluorine-containing electrolyte** **Toxic metal (Co)**

References

[1] M. J. Frisch, G. W. Trucks, H. B. Schlegel, *et al.*, *Gaussian 16*, Revision C.01, Gaussian, Inc., Wallingford CT, **2016**.

[2] W. F. Humphrey, A. Dalke and K. Schulten, *J. Mol. Graph.*, **1996**, 14 1, 33-38

[3] D. Van Der Spoel, E. Lindahl, B. Hess, G. Groenhof, A. E. Mark, H. J. Berendsen, *J. Comput. Chem.,* **2005**, 26, 1701-1718.

[4] L. Monticelli, S. K. Kandasamy, X. Periole, R. G. Larson, D. P. Tieleman, S. J. Marrink, *J. Chem. Theory Comput.,* **2008**, 4, 819-834.

[5] S. J. Marrink, H. J. Risselada, S. Yefimov, D. P. Tieleman, A. H. De Vries, *J. Phys. Chem. B.,* **2007**, 111, 7812-7824.

[6] Y. Yang, N. Fu, Q. Dong, M. Li, J. Li, C. Li, Z. Wei, *Adv. Mater. Interfaces,* **2020**, 7.

[7] D. Frenkel, B. Smit, Understanding molecular simulation: From algorithms to applications (1996).

[8] W. Humphrey, A. Dalke, K. *Schulten, J. Mol. Graph.*, **1996**, 34, 33-38.

[9] S. Matteson, E. Williams, *Energy Policy,* **2015**, 85, 71-79.

[10] M. Gutsch, J. Leker, *Appl. Energy,* **2024**, 353, 122-132.